Time-resolved secondary emission from three-level electron-phonon coupled systems: Numerical study of radiative and nonradiative transitions

Masato Suzuki and Takeshi Iida
Department of Physics, Faculty of Science, Osaka City University, Sumiyosi-ku, Osaka, 558, Japan
(Received 5 August 1996; revised manuscript received 9 May 1997)

The spectral structures of the transient resonant secondary emission are investigated in a three-level electron-phonon coupled system in order to clarify dynamical properties of the nonradiative transitions occurring in the crossing region of the potential-energy curves. The time-resolved resonant secondary-emission spectra are calculated for an instantaneous excitation pulse; in the calculation, we take into account the uncertainty relation between energy and time for emission processes by introducing explicitly a temporal form of the resolution function of the measurement system. The time evolution of the excited state is solved numerically by using the real-time Trotter's formula, without assuming any *a priori* trajectories. We study how the lattice relaxation and the nonradiative transition contribute to the processes of secondary emissions by analyzing the temporal behaviors of the emission spectra. It is found that, in addition to the peaks due to the radiative transitions from the excited states during the lattice relaxation, the oscillatory structures appear in the spectra in the energy domain, which is due to the quantum-mechanical interference effects of the excited states in the potential crossing region. [S0163-1829(98)09301-1]

I. INTRODUCTION

Recent development of measurement techniques using the femtosecond laser has made it possible to investigate various kinds of ultrafast phenomena which occur in condensed matter. The transient resonant secondary emission is one of the typical phenomena. The time-resolved spectroscopy of the resonant secondary emission provides us with information to obtain a deeper understanding of relaxation and dynamical processes in the optically excited states.[1–4] In the present work, we study the transient resonant secondary emission in a three-level electron-phonon coupled system to clarify how the characteristic features of the dynamical processes which occur in the level-crossing region are reflected in the spectral structures of the transient secondary emission. The dynamical aspects of the nonradiative transition in a similar system have been studied by Nasu and Kayanuma.[5–7] They have calculated the temporal behavior of the nonradiative transition and the time-integrated intensity of the secondary emission, and also clarified the conditions under which the Landau-Zener formula is valid.

In localized electron-phonon coupled systems such as impurity or defect states in solids, the excited state of the localized electron may interact with other excited states which belong to a different configuration of atoms in the localized region. The interaction causes a nonradiative transition from one electronic state to another in the crossing region of the respective potential curves with the time interval as short as the lattice relaxation time; this transition is called the nonadiabatic transition with the emphasis on the dynamical aspects of the nonradiative transitions. The nonadiabatic transition is one of fundamental mechanisms which govern the state or structural change of a system in various fields of physics and chemistry. In condensed matter, the most typical examples are the luminescence quenching of the F centers, and the polarization correlation between the absorption and the emission in Tl-like centers.[5–7] In molecular systems, there are various types of examples; photodissociation, photoisomerism, chemical reactions, the elimination of molecules adsorbed on a solid surface, and so forth.[8] The essential underlying physics in these phenomena is the same as that in our three-level electron-phonon coupled system.

Let us see the schematic feature of the potential energy curves of the three-level electron-phonon coupled systems. One of the typical cases is shown in Fig. 1 as a function of a configuration coordinate ($\equiv Q$). Q represents a collective motion of atoms. In this figure, $|0\rangle$ denotes the initial ground state. $|1\rangle$ and $|2\rangle$ are the excited states. We call these poten-

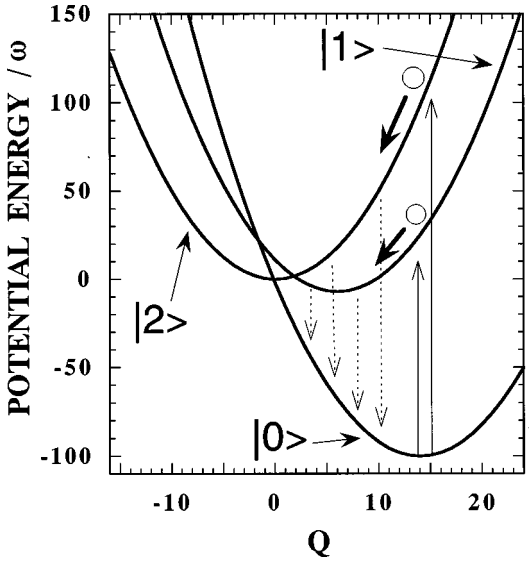

FIG. 1. Diabatic potential curves of the three-level system as a function of a configuration coordinate Q for the parameter values; $\varepsilon_0/\omega=-100$, $\varepsilon_1/\omega=-7$, $\varepsilon_2/\omega=0$, $\beta_0/\omega=98$, $\beta_1/\omega=18$, and $\beta_2/\omega=0$. $|0\rangle$ denotes the initial ground state. $|1\rangle$ and $|2\rangle$ are the photoexcited states from $|0\rangle$.

tials *diabatic potential curves*. They interact with each other in the vicinity of the potential crossing point. Under the limit of the adiabatic approximation for Q, they are split into two curves which are commonly called *adiabatic potential curves*.[9] If the Franck-Condon state is created in $|1\rangle$ by the optical excitation from $|0\rangle$, it will propagate along the potential curve of $|1\rangle$. Then, it may pass through the crossing point of the potential curves $|1\rangle$ and $|2\rangle$. Around this point, the nonradiative electronic transition occurs and the component of excited state $|2\rangle$ is constructed during the lattice relaxation.

The essential features of such dynamical processes occurring in the potential crossing systems are summarized as follows. (1) Because the change in the electronic states occurs during the motion of atoms described by Q, the nonadiabaticity plays an important role in every step of the transition. (2) As discussed above, when the Franck-Condon excited state passes through the potential crossing region before the transition to the ground state emitting the photon, the different components of the excited state are created on the potential curves due to the nonradiative transition. This brings about the quantum-mechanical interference effects between these components. (3) Because the slopes of the tangents of these potentials are different from each other at the crossing region, the electronic transition is accompanied by the changes in the motion of atoms. Therefore, a back reaction from the electronic transition to the atomic motion is also the essential feature.

In Sec. II, we introduce a model Hamiltonian of the three-level electron-phonon coupled system, and derive the formal expression for the time-resolved resonant secondary-emission spectrum. In Secs. III and IV, we carry out the numerical calculation on the basis of the Trotter's formula and investigate how the above-mentioned dynamical features appear in the secondary-emission spectra.

II. MODEL HAMILTONIAN OF THREE-LEVEL SYSTEM AND EXPRESSION FOR TIME-RESOLVED SECONDARY-EMISSION SPECTRUM

To describe our system, we adopt a model Hamiltonian $(\equiv H)$ $(\hbar=1)$:

$$H=\sum_{i=0,1,2} H_i+V, \tag{2.1}$$

$$H_i=\left[\varepsilon_i+\frac{\omega}{2}\left\{-\frac{\partial^2}{\partial Q^2}+(Q-\sqrt{2\beta_i/\omega})^2\right\}\right]a_i^\dagger a_i, \tag{2.2}$$

$$V=Ta_1^\dagger a_2+\text{H.c.} \tag{2.3}$$

Here, $a_i^\dagger(a_i)$ denotes the creation (annihilation) operator for the ith electronic state with an energy ε_i, where the ground state is designated by $i=0$, the excited states by $i=1$ and 2. They satisfy $\Sigma_i a_i^\dagger a_i=1$. Q is the dimensionless coordinate of the motion of atoms, along which the lattice relaxation of the center-of-mass motion of the Franck-Condon excited state occurs. Since the nonradiative transition is expected to occur only in the vicinity of the crossing point, we approximate the potential for Q to be harmonic with a curvature ω, neglecting its anharmonicity as shown in Fig. 1; for instance, in condensed matter the typical value of the frequency ω is of the order of a few hundred cm^{-1}. V is the interaction Hamiltonian, wherein the nonradiative electronic transition is assumed to occur only in the excited states. T is the resonance transfer integral of the electron between two excited states. Strictly speaking, T may depend on Q. However, in this study, its dependence is not taken into account. In the case of T having the same order of magnitude as ω, the characteristic time of the nonradiative transition becomes comparable with the lattice relaxation time, and then the interaction between the dynamical motions of electron and lattice plays an essential role. The parameters β_i give the shift of the equilibrium position of Q as shown in Fig. 1, which comes from the electron-lattice interactions. This effect brings about the change of the equilibrium configuration of atoms when the radiative or the nonradiative transition of electrons takes place.

The Schrodinger equation

$$H_i|\varphi_{in}\rangle=\varepsilon_{in}|\varphi_{in}\rangle, \tag{2.4}$$

can easily be solved; the vibronic state $|\varphi_{in}\rangle$ with the eigenvalue ε_{in} is given by the product $|i\rangle|\chi_n^i\rangle$, $|\chi_n^i\rangle$ being the nth-phonon state appropriate to the ith electronic state $|i\rangle$. The total wave function $[\equiv|\Psi(t)\rangle]$ is constructed by the linear combination of these vibronic states as follows:

$$|\Psi(t)\rangle=\sum_{i,n} C_{in}(t)|\varphi_{in}\rangle, \tag{2.5}$$

where $C_{in}(t)$ is the time-dependent coefficient.

Time developments of the occupancies in each electronic state are defined by the trace of the density operator $[\equiv\rho(t)=|\Psi(t)\rangle\langle\Psi(t)|]$ as

$$\rho_i(t)=\text{Tr}_i[\rho(t)], \tag{2.6}$$

where Tr_i means the diagonal sum for all over the phonon states in the ith electronic state.

Let us derive the expression for the time-resolved spectrum of resonant secondary emission adapted to our model system. The general formula has been derived by Aihara and Kotani,[1] which is given by the four-time correlation function of the dipole moments. In the derivation, they properly take into account the uncertainty relation between energy and time by introducing explicitly the temporal forms of the incident-photon wave packet $[\equiv F_a(t)]$ and the resolution function of the measurement system $[\equiv F_e(t)]$. Applying the general formula to our model system and decomposing the correlation function into the correlated absorption and emission form, we get the expression for the time-resolved spectrum $[\equiv S(\Omega_a,\Omega_e,t_e)]$ as

$$\begin{aligned}S(\Omega_a,\Omega_e,t_e)=&\int_{-\infty}^{\infty}dt_s\int_{-\infty}^{\infty}d\mu\int_0^{\infty}d\tau_0\int_{\mu-2\tau_0}^{\mu+2\tau_0}d\sigma\\&\times F_a(t_s-\tau_0+\sigma/2)F_a(t_s-\tau_0-\sigma/2)\\&\times F_e(t_e-t_s-\mu/2)F_e(t_e-t_s+\mu/2)\\&\times\text{Tr}[\exp(iH\tau_0)B(\Omega_e,\mu)\\&\times\exp(-iH\tau_0)A(\Omega_a,\sigma)],\end{aligned} \tag{2.7}$$

where

$$A(\Omega_a,\sigma)\equiv\exp(iH\sigma/2)M_a^\dagger\exp[-i(H+\Omega_a)\sigma]\rho_0 M_a \times\exp(iH\sigma/2), \tag{2.8}$$

$$B(\Omega_e,\mu)\equiv\exp(iH\mu/2)M_e^\dagger\exp[-i(H+\Omega_e)\mu]M_e \times\exp(iH\mu/2). \tag{2.9}$$

Here, Ω_a and Ω_e are the mean energies of the incident- and the detected-photon pulses, respectively. The time t_e is the mean photon emission time when putting $t=0$ at the mean time of the incident photon pulse. ρ_0 is the density operator for the initial state of whole system. The operators $A(\Omega_a,\sigma)$ and $B(\Omega_e,\mu)$ represent the absorption and the emission processes, respectively, and τ_0 is associated with the time interval between them. The propagator $\exp(-iH_i\tau_0)$ represents the time evolution in the excited subspace. M_a and M_e denote the dipole moments of absorption and emission, respectively. In our model, both $|1\rangle$ and $|2\rangle$ are assumed to be optically allowed, then M_a and M_e are written as

$$M_a^\dagger=M_e^\dagger=\sum_{m,n}|\varphi_{1m}\rangle S_{m,n}^{(1)}\langle\varphi_{0n}|+\sum_{m,n}|\varphi_{2m}\rangle S_{m,n}^{(2)}\langle\varphi_{0n}|, \tag{2.10}$$

where, $S_{m,n}^{(i)}$ denotes the overlap integral of phonon wave functions, $S_{m,n}^{(i)}=\langle\chi_m^i|\chi_n^0\rangle$, $i=1,\ 2$.

Equation (2.7) is simplified by introducing the following assumptions: (i) The incident pulse is supposed to be the white pulse, that is, $F_a(t)=\delta(t)$; (ii) The temporal forms of the resolution function of measurement system have the Gaussian profile, $F_e=(\delta_e^2/\pi)^{1/4}\exp(-\delta_e^2t^2/2)$, under the assumption of the minimum uncertainty between energy and time; (iii) The time interval during the absorption or the emission process is assumed to be sufficiently short as compared with the time interval discussed in this study. Therefore, in Eqs. (2.8) and (2.9), V can be ignored and only H_i's contribute to the time evolution of the system during the absorption or the emission; and (iv) We consider the case where the temperature of the system is 0 K, so ρ_0 can be set to be $|\varphi_{00}\rangle\langle\varphi_{00}|$.

Under these assumptions, carrying out the time integrals for t_s, μ, and σ, we arrive at the desired expression of spectrum $[\equiv S(\Omega_e,t_e)]$ as

$$S(\Omega_e,t_e)=4\sqrt{\pi}\int_0^\infty d\tau_0\ \exp[-\delta_e^2(\tau_0-t_e)^2] \times\langle\Psi(\tau_0)|B(\Omega_e)|\Psi(\tau_0)\rangle, \tag{2.11}$$

with

$$B(\Omega_e)=\sum_{m,n,i=1,2}|\varphi_{i,m}\rangle F_{m,n}^{(i)}(\Omega_e)\langle\varphi_{i,n}| +\sum_{m,n}|\varphi_{1,m}\rangle F_{m,n}^{(1-2)}(\Omega_e)\langle\varphi_{2,n}|, \tag{2.12}$$

where

$$F_{m,n}^{(i)}(\Omega_e)=\sum_r S_{m,r}^{(i)}S_{n,r}^{(i)} \times\exp\left[-\frac{1}{\delta_e^2}\left(\frac{\varepsilon_{i,m}+\varepsilon_{i,n}}{2}-\varepsilon_{0,r}-\Omega_e\right)^2\right], \tag{2.13}$$

$$F_{m,n}^{(1-2)}(\Omega_e)=2\sum_r S_{m,r}^{(1)}S_{n,r}^{(2)} \times\exp\left[-\frac{1}{\delta_e^2}\left(\frac{\varepsilon_{1,m}+\varepsilon_{2,n}}{2}-\varepsilon_{0,r}-\Omega_e\right)^2\right]. \tag{2.14}$$

The function $F_{m,n}^{(i)}(\Omega_e)$ corresponds to the diagonal part of the emission intensity, which gives the emission spectra from the ith electronic state $[\equiv S_i(\Omega_e,t_e)]$. $F_{m,n}^{(1-2)}(\Omega_e)$ is the off-diagonal part, which gives the interference effects in the emission associated with $|1\rangle$ and $|2\rangle$ $[\equiv S_{12}(\Omega_e,t_e)]$.

When the excitation pulse is the white light as supposed above, the initial excited state $[\equiv|\Psi(0)\rangle]$ is nothing but the Franck-Condon state, and is given by the coherent state in the Q space. The time development of $|\Psi(0)\rangle$ up to t is calculated numerically by using the real time Trotter's formula together with Eq. (2.1),

$$|\Psi(t)\rangle=\exp(-iHt)|\Psi(0)\rangle =\lim_{L\to\infty}\{e^{-iH_1t/L}\times e^{-iH_2t/L}\times e^{-iVt/L}\}^L|\Psi(0)\rangle. \tag{2.15}$$

In general, the initial coherent-state oscillates along the potential curve and will relax down to the equilibrium point. We are interested in the dynamical processes which occur before the relaxation. In order to focus only on such a dynamical process, we deal with the first period of the reciprocating motion of the coherent state, that is $0\leqslant t\leqslant 2\pi/\omega$. For the same reason, the damping mechanism of the center-of-mass motion of the excited wave packet is not included in our model.

We can easily see that the present calculation fully takes the aforementioned effects; the nonadiabaticity, the quantum-mechanical interference, and the quantum-mechanical back reaction from the electronic transition to the atomic motion.[10,11]

III. ONE-LEVEL EXCITATION CASE

As one of the typical cases, we have chosen a set of parameter values as $\varepsilon_0/\omega=-100$, $\varepsilon_1/\omega=-7$, $\varepsilon_2/\omega=0$, $\beta_0/\omega=98$, $\beta_1/\omega=18$, and $\beta_2/\omega=0$. The diabatic potential curves for these parameter values are depicted in Fig. 1. The number of phonon states is taken into account up to 150 in each electronic state. Such a size of phonon space is large enough to construct the excited wave packets and to describe their time propagations.

In order to make the analysis clear, at first we discuss the hypothetical one-level excitation case where the wave packet is supposed to be excited only on the potential curve $|1\rangle$, but

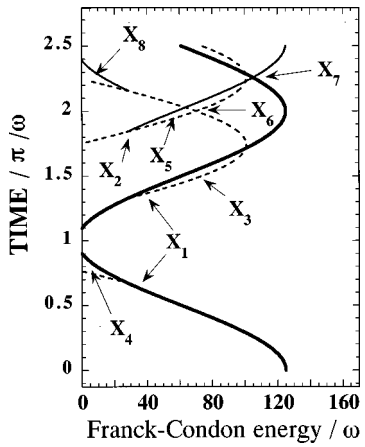

FIG. 2. The classical trajectory of center-of-mass motion of the excited wave packet on the diabatic potential curves in time and Franck-Condon energy space for one-level excitation case. Solid (dotted) line corresponds to the classical trajectory on the potential curve of $|1\rangle$ ($|2\rangle$).

the emission is allowed from $|1\rangle$ and $|2\rangle$. Subsequently, on the basis of the analysis of the one-level excitation case, we will discuss a more actual case where the wave packets are simultaneously photocreated on both potential curves $|1\rangle$ and $|2\rangle$.

It is useful for the subsequent discussion to visualize the time evolution of the optically excited wave packet in the one-level excitation case. The classical motion of the center-of-mass of the wave packet on the diabatic potential curves is represented by plotting the corresponding Franck-Condon energies in the energy-time domain as shown in Fig. 2. We call the path in the energy-time domain a *classical trajectory*.

In Fig. 2, the solid (dotted) line represents the classical trajectory for the motion of wave packet on the potential curve $|1\rangle$ ($|2\rangle$). The branch points of the solid and dotted lines, X_1, X_2, and X_8, indicate the change of electronic states of the classical trajectories due to the nonradiative transitions between $|1\rangle$ and $|2\rangle$ which occur in the potential crossing region. Quantum mechanically, it is possible for the wave packet to travel along both trajectories when crossing through the branch point. On the other hand, the crossings of the same kind of lines, X_6 and X_7, represent the classical trajectories for the collision between the two components of wave packet belonging to the same electronic state, which have been created through the nonradiative transitions in the crossing region during the reciprocating motion of the wave packet.

A. Nonradiative transition

First, let us study the time evolution of the electron occupancy in $|1\rangle$, $\rho_1(t)[=1-\rho_2(t)]$ for the one-level excitation case. The occupancy $\rho_1(t)$ computed by using Eqs. (2.6) and (2.15) is shown in Fig. 3 as a function of time up to $t=2.5\pi/\omega$ for various values of T; $T/\omega=0.5$ (a), 1.0 (b), and 1.5 (c).

From the figure, we can see that the nonradiative transition from $|1\rangle$ to $|2\rangle$ occurs at $t\sim 0.7\pi/\omega$ and $1.3\pi/\omega$. These transition points correspond to the mean times when the initial wave packet passes through the relevant potential crossing region. The classical trajectories for these transitions are indicated by the branch points X_1 in Fig. 2.

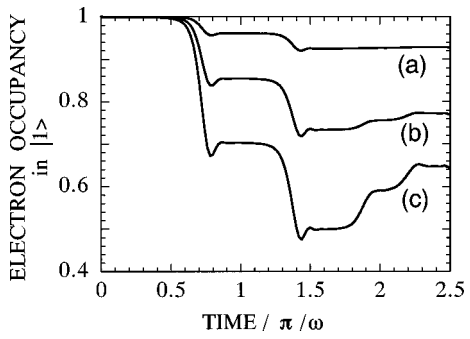

FIG. 3. Time evolution of the electron occupancy in the state $|1\rangle$, $\rho_1(t)[=1-\rho_2(t)]$, for the case of the one-level excitation. (a) $T/\omega=0.5$, (b) 1.0, (c) 1.5.

In case (a) in Fig. 3, even though a small amount of the transition from $|1\rangle$ to $|2\rangle$ is observed at $t\sim 0.7\pi/\omega$ and $1.3\pi/\omega$, there is no increase of $\rho_1(t)$, that is, no backward electron transfer from $|2\rangle$ to $|1\rangle$ takes place. This behavior means that the Franck-Condon state excited in $|1\rangle$ moves mainly along the potential curve $|1\rangle$ and the nonradiative transition at the crossing region is well described by the Landau-Zener formula.[12] On the other hand, in cases (b) and (c) the backward electron transfer from $|2\rangle$ to $|1\rangle$ becomes remarkable in the vicinity of $t=1.8\pi/\omega$, and $2.2\pi/\omega$. These transition points correspond to the classical trajectories indicated by X_2 and X_8 in Fig. 2. The existence of the backward transfer means that there is a component of the excited wave packet moving mainly along the adiabatic potential curve. That is, the adiabatic picture becomes more adequate as increasing T. Comparing curves (a), (b), and (c), we can see how the backward electron transfer increases with increasing T. The set of the parameters used in calculations gives the intermediate case where the adiabatic and diabatic processes coexist in the nonradiative transitions.

B. Time-resolved resonant secondary-emission spectra

With using Eqs. (2.11) and (2.15), the time-resolved secondary-emission spectra are computed for various times up to $t=\frac{9}{4}\pi/\omega$. The results are shown in Fig. 4, where the parameter values are fixed as $\delta_e^{-1}=\frac{1}{4}\pi/\omega$ and $T/\omega=1.5$. As mentioned just below Eq. (2.14), the emission spectra consist of three components; the emission $S_i(\Omega_e,t_e)$ $(i=1,2)$, due to the transition from $|i\rangle$ and that of $S_{12}(\Omega_e,t_e)$ which comes from the interference between the two processes via states $|1\rangle$ and $|2\rangle$. In Fig. 4, the components S_1, S_2, and S_{12} are presented, respectively, in (a), (b), and (c) together with the total emission $S(\Omega_e,t_e)=S_1+S_2+S_{12}$ in (d).

Let us discuss how the dynamical behaviors of the wave packet is reflected in the spectral structures of the secondary emission with the help of the classical trajectories discussed above.

From Fig. 4, we can see that $S(\Omega_e,t_e)$ is mainly determined by the two components $S_1(\Omega_e,t_e)$ and $S_{12}(\Omega_e,t_e)$. In accordance with the motion of the Franck-Condon excited state passing through the potential curve of $|1\rangle$, the peak of the emission from $|1\rangle$ shows the oscillatory behavior in the

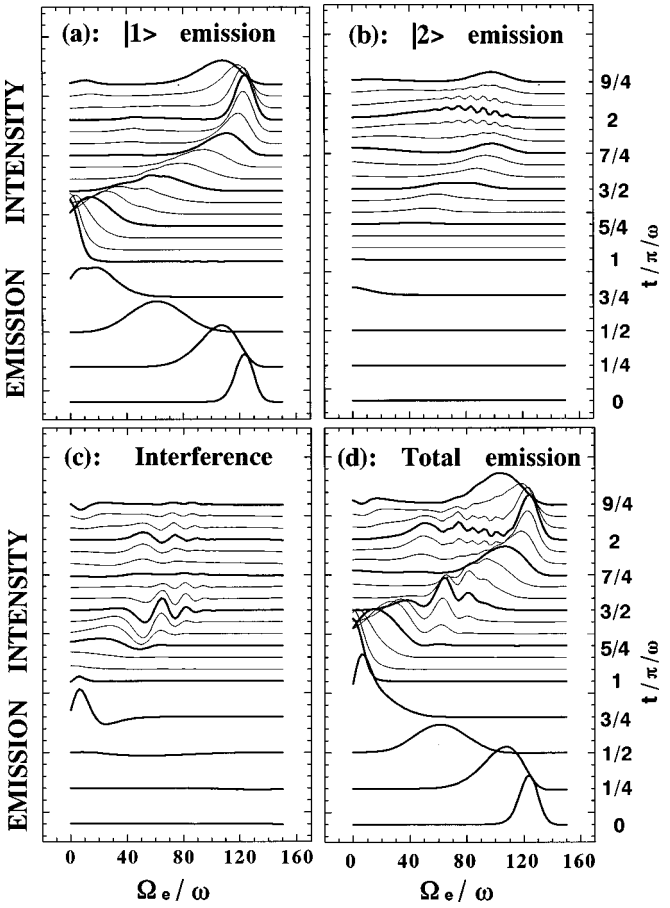

FIG. 4. Time-resolved emission spectra as a function of Ω_e for $T/\omega=1.5$ in the one-level excitation case. (a) the emission spectra from $|1\rangle[\equiv S_1(\Omega_e,t_e)]$, (b) from $|2\rangle[\equiv S_2(\Omega_e,t_e)]$, (c) the interference spectra in the emitted photon associated with $|1\rangle$ and $|2\rangle$ $[\equiv S_{12}(\Omega_e,t_e)]$, (d) the total emission intensity $[\equiv S(\Omega_e,t_e)]$. δ_e^{-1} is set to be $\frac{1}{4}\pi/\omega$.

energy-time domain as shown in Fig. 4(a). This oscillation is appreciated by the classical trajectory depicted by the thick curve in Fig. 2. In Fig. 4(c), the spectra have an oscillatory structure with respect to the emission energy in the vicinity of $\Omega_e=60\omega$ and $t=1.5\pi/\omega$. This is considered to originate from the interference in the emitted photon associated with the following two components of the wave packet: one is created in $|2\rangle$ from $|1\rangle$ through the nonradiative transition that occurs at $t\sim 1.3\pi/\omega$, and the other is left in $|1\rangle$ without making the transition. The classical trajectories corresponding to these propagating components are indicated by X_3 in Fig. 2. Because this interference appeared just behind the nonradiative electronic transition, it should directly reflect the transition occurring in the potential crossing region. As shown in Fig. 4(c), the same kind of interference spectrum is observed in the vicinity of $\Omega_e=20\omega$ and $t=\frac{3}{4}\pi/\omega$. The corresponding classical trajectories for the propagating wave packet are indicated by X_4. Moreover, in Fig. 4(c) the other oscillatory structure is observed in the vicinity of $\Omega_e=60\omega$ and $t=2\pi/\omega$. This structure is due to interference in the emitted photon associated with the following two components of wave packet: one is created in $|1\rangle$ from $|2\rangle$ through the nonradiative transition occurring at $t\sim 1.7\pi/\omega$, and the other remains in $|2\rangle$ without making the transition at this

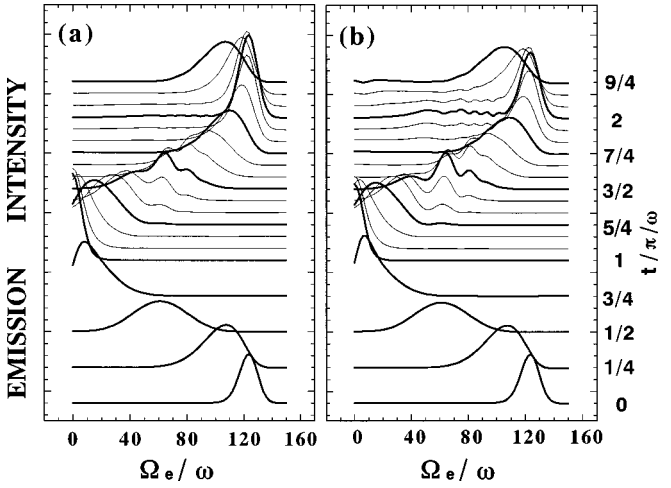

FIG. 5. Time-resolved total emission spectra as a function of Ω_e for $\delta_e^{-1}=\frac{1}{4}\pi/\omega$ in the one-level excitation case. (a) $T/\omega=0.5$, (b) 1.0.

time. This oscillatory structure directly reflects the backward electron transfer from $|2\rangle$ to $|1\rangle$. The classical trajectories related to the components that give this interference are indicated by X_5. It should be noted that the phase of the oscillation around the point X_5 is completely reverse from that occurring in X_3, which will be discussed in detail in the subsequent section.

Although the emission $S_2(\Omega_e,t_e)$ has very small intensity, as shown in Fig. 4(b), it has oscillatory structures with respect to the emission energy in the vicinity of $\Omega_e=90\omega$ and $t=2\pi/\omega$. This oscillation originates from the interference in the emission associated with the two components in $|2\rangle$ generated through the nonradiative transitions at $t\sim 0.7\pi/\omega$ and $t\sim 1.3\pi/\omega$. These two components propagate separately along the potential curve of $|2\rangle$. Then, they collide with each other near $\Omega_e=90\omega$ and $t=2\pi/\omega$, whose classical trajectories are indicated by X_6 in Fig. 2. Quantum mechanically, it corresponds to the interference between the two components in the same electronic state. The period of its oscillation in $S_2(\Omega_e,t_e)$ is approximately one-half of that in $S_{12}(\Omega_e,t_e)$; the reason of this is also considered in the subsequent section. As shown in Fig. 4(d), these oscillatory structures due to the interference effects clearly appear in the spectral shape of $S(\Omega_e,t_e)$ at the corresponding energy-time regions.

In order to see the effects of T on the emission spectra, we show the total emission intensities for the cases of $T/\omega=0.5$ and 1.0 in Fig. 5(a) and 5(b), respectively. The other parameters are the same as in Fig. 4. As shown in Fig. 3, when T increases from a value of the nearly diabatic case, the transition from $|1\rangle$ to $|2\rangle$ increases due to the enlargement of the adiabatic character in the transition, and furthermore the backward transition from $|2\rangle$ to $|1\rangle$ becomes significant. These effects make the spectral structures more complicated. Especially, the oscillatory structures in the spectra become more clear.

Let us show the time-integrated total emission intensity, $S_t(\Omega_e)=\int_0^{2\pi/\omega}S(\Omega_e,t)dt$, in Fig. 6 for $\delta_e^{-1}=\frac{1}{4}\pi/\omega$ as a function of Ω_e for the various values of T; $T/\omega=0.5$ (a), 1.0 (b), and 1.5 (c). There are two peaks in the vicinity of $\Omega_e=5\omega$ and 120ω, which correspond to the emission from

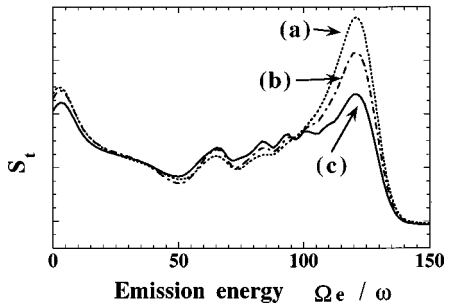

FIG. 6. Time-integrated total emission spectrum as a function of Ω_e for $\delta_e^{-1}=\frac{1}{4}\pi/\omega$ in the one-level excitation case for various values of T. (a) $T/\omega=0.5$, (b) 1.0, (c) 1.5.

the wave packet propagating near the turning points on the potential curve $|1\rangle$. Near the turning point, the mean velocity of the center-of-mass motion of the wave packet tends to zero and the wave packet stays for a long time in the corresponding energy region. This causes the two peaks in the emission spectra. On the other hand, two types of oscillatory structures are clearly observed in the energy range between the peaks. They come from the interference effects which occur when the wave packet passes through the potential crossing region during the lattice relaxation as discussed before. These facts indicate the possibility that even in the time-integral emission spectra obtained by stationary measurements, we can observe the remarkable structures in the energy domain which reflect the dynamical behavior of the optically excited state.

C. Interference effects

Let us discuss in detail the interference effects on the oscillatory structures appearing in the energy-time domain indicated by the classical trajectories near X_3, X_5, and X_6 in Fig. 2. In general, the presence of the oscillations in the emission spectra with respect to the energy means that there are some characteristic times in the emission process in the sense of the Fourier transform between energy and time. If there is any difference in the emission time associated with the different components of the wave packet, the emission spectra may have oscillatory structures with respect to the emission energy.

Let us discuss the origin of such a time difference in our system by simplifying the emission processes as follows. In Fig. 7, we schematically show the classical trajectories of the region of X_3; t_e denotes the emission time, and P_1 and P_2 are the positions of the components of wave packet in the energy-time domain at t_e. The resolution function of the measurement system is schematically displayed on the time and energy axes. When we observe the emission with energy Ω_e at t_e, the photon will be emitted from the energy-time domain P_1' and P_2', because the wave packet can propagate from $P_1(P_2)$ to $P_1'(P_2')$ within the time interval of δ_e^{-1}. This process brings about the two characteristic times in the emission process, $\tilde{t}_1$ and $\tilde{t}_2$; here $\tilde{t}_1$ and $\tilde{t}_2$ are the times when the components of wave packets reach the positions P_1' and P_2', respectively. Under these arguments, we define the time difference in the emitted photon $[\equiv\Delta t(\Omega_e)]$ by the time interval between P_1' and P_2' as shown in Fig. 7. $\Delta t(\Omega_e)$ causes

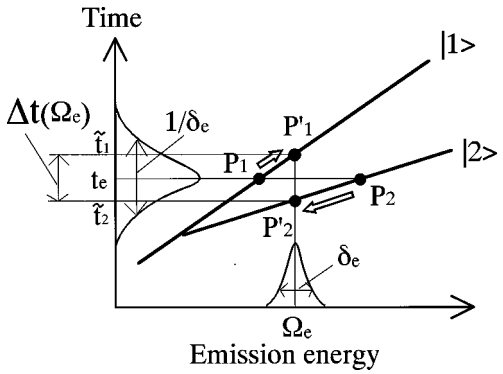

FIG. 7. Schematic curves of the classical trajectories at the region of X_3. t_e denotes the emission time. P_1 and P_2 are the positions of the center-of-mass of the components of the wave packet in the energy-time domain at t_e, and P_1' and P_2' are that of the wave packets in the energy-time domain at Ω_e. $\tilde{t}_1$ and $\tilde{t}_2$ are the corresponding times at the positions of P_1' and P_2', respectively.

the oscillatory behavior with respect to the emission energy through the interference. This is one of the dynamical effects on the emission processes, peculiar to level crossing systems.

Applying these assumptions to Eq. (2.7), we can derive the simple expression for the interference intensity $[\equiv I_{\rm int}(\Omega_e,t_e)]$ that holds for near the potential crossing region as

$$I_{\rm int}(\Omega_e,t_e)\sim C_1^*(\tilde{t}_1)C_2(\tilde{t}_2)e^{-i\Omega_e\Delta t(\Omega_e)}F_e(\tilde{t}_1-t_e)F_e(\tilde{t}_2-t_e)+\text{c.c.} \tag{3.1}$$

Here, $C_1(\tilde{t})$ and $C_2(\tilde{t})$ are the time-dependent coefficients for the electronic states $|1\rangle$ and $|2\rangle$, respectively. They include information about the phase of the electron, together with the electron occupancy in each electronic state at $\tilde{t}$. In order to focus on the interference effects, only the phase of the electronic state is taken into account as $C_1(t)\sim e^{in_1\pi}$ or $C_2(t)\sim e^{in_2\pi}$; n_1 and n_2 denote the phases of the electronic states of the components of the wave packet. Under these simplifications, $I_{\rm int}(\Omega_e,t_e)$ is written as

$$I_{\rm int}(\Omega_e,t_e)\sim e^{i(n_2-n_1)\pi}\cos(\Omega_e\Delta t(\Omega_e))\times F_e(\tilde{t}_1-t_e)F_e(\tilde{t}_2-t_e). \tag{3.2}$$

In the above equation, the term $\cos(\Omega_e\Delta t(\Omega_e))$ determines the period of the oscillation; with increasing $\Delta t(\Omega_e)$, the period of the oscillation with respect to Ω_e becomes shorter. As seen in Fig. 2, $\Delta t(\Omega_e)$ near X_6 is larger than these near X_3 and X_5. This causes the period of the oscillation in $S_2(\Omega_e,t_e)$ at X_6 to be approximately one-half of that in $S_{12}(\Omega_e,t_e)$ at X_3 and X_5. The $F_e(\tilde{t}_1-t_e)F_e(\tilde{t}_2-t_e)$ term determines the energy region of the oscillation through the width of $1/\delta_e$. The term of $e^{i(n_2-n_1)\pi}$ in Eq. (3.2) determines the phase of the oscillatory structure in the interference emission spectra.

In order to see the phase of the electronic state of the propagating wave packet, let us consider the phase change due to the nonradiative transition occurring in the potential crossing region. In Fig. 8, the two diabatic potential curves, $|1\rangle$ and $|2\rangle$, are depicted schematically by solid lines; they cross each other at Q_0. When the interlevel interaction T is

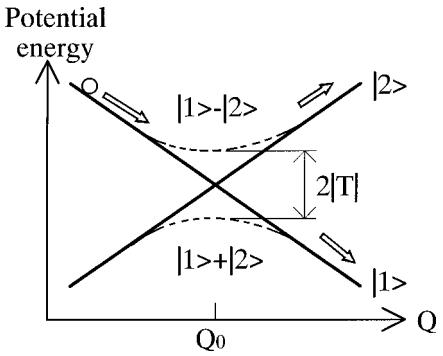

FIG. 8. Schematic curves for diabatic potential energies of $|1\rangle$ and $|2\rangle$ (solid lines), and for adiabatic potential energies of $|1\rangle+|2\rangle$ and $|1\rangle-|2\rangle$ (dotted lines).

taken into account in the adiabatic approximation, the diabatic potentials are split into the adiabatic potential curves with the energy gap of $2|T|$ at Q_0, which are represented by dotted lines. When T is a negative (positive) value, the electronic state of the lower adiabatic curve is constructed by $|1\rangle+|2\rangle(|1\rangle-|2\rangle)$, and the upper curve by $|1\rangle-|2\rangle(|1\rangle+|2\rangle)$. In this situation, we consider the case where the wave packet approaches the crossing region from the left side of the potential of $|1\rangle$. If the wave packet passes through the crossing region without transition, of course, the phase of the electronic state should be kept unchanged. However, when the transition from $|1\rangle$ to $|2\rangle$ occurs, the transferred components of wave packet may pass through the crossing region being affected by the upper curve of the adiabatic potential, $|1\rangle-|2\rangle$, and then it tends to the diabatic curve $|2\rangle$. In this case, the phase of the state $|2\rangle$ of the adiabatic potential curve $|1\rangle-|2\rangle$ is maintained even in the region far from the crossing point. Therefore, the electronic state of the wave packet has the phase shift as $e^{i\pi}$ due to the nonradiative transition. On the other hand, when the wave packet approaches the crossing region from the right side of $|1\rangle$, there is no such phase shift in the transition from $|1\rangle$ to $|2\rangle$, because the relevant adiabatic potential curve is the lower one, $|1\rangle+|2\rangle$.

Let us return to the three-level system, and determine the phase of the propagating wave packet based on the above-mentioned argument. In Fig. 9, we write the values of the electronic phase of each wave packet propagating on the classical trajectories depicted in Fig. 2. In this figure, it should be noted that in our numerical calculation T is set positive.

From this figure, we can see that the components of wave packet propagating in the regions of X_3 and X_8 have the same phase, and those in X_4 and X_5 have different phases. As discussed in Fig. 4(c), the oscillatory structures of the interference occurring in the regions of X_3 and X_5 have the inverse phases of each other, because $e^{i(n_2-n_1)\pi}$ is equal to $+1$ and -1 in the regions of X_3 and X_5, respectively.

As seen above, the oscillatory structures of the emission spectra due to the interference effects appearing in X_3, X_5, and X_6 give information about the dynamical nature of the nonadiabatic transitions in the excited state. A detailed analysis of the emission from the wave packet just after and/or before the nonadiabatic transition are subjects for a future study.

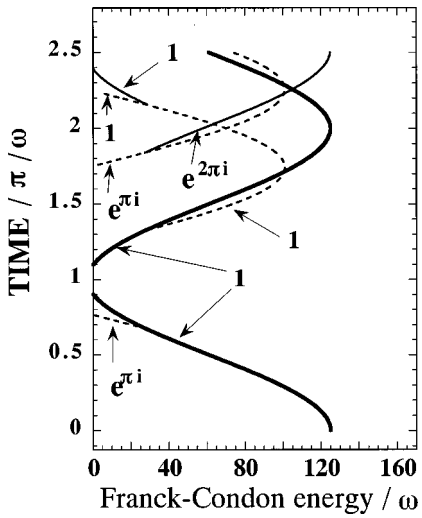

FIG. 9. The phase of the electronic state of propagating components of the wave packet on the classical trajectories. T is set positive in our numerical calculations.

IV. TWO-LEVEL EXCITATION CASE

Let us proceed to the two-level excitation case where both $|1\rangle$ and $|2\rangle$ are excited simultaneously from $|0\rangle$ by the white light pulse. We adopt the three-level system with the same parameter values as in the one-level excitation case.

The time evolution of the electron occupancy in $|1\rangle$, $\rho_1(t)$, is shown in Fig. 10 as a function of time, where (a), (b), and (c) correspond to the cases of $T/\omega=0.5$, 1.0, and 1.5, respectively. δ_e^{-1} is set to be $\frac{1}{4}\pi/\omega$. Observing the figure, we can see following facts. The Franck-Condon states created simultaneously in both $|1\rangle$ and $|2\rangle$ by the optical excitation propagate almost independently along the respective potential curves except the potential crossing region. In the crossing region, reflecting the nonradiative transition from $|1\rangle$ to $|2\rangle$ for the photoexcited component in $|1\rangle$, $\rho_1(t)$ decreases in the vicinity of $t=0.7\pi/\omega$ and $1.3\pi/\omega$. This is the same as discussed in the one-level excitation case. On the other hand, $\rho_1(t)$ increases in the vicinity of $t=0.4\pi/\omega$ and $1.6\pi/\omega$. These transition points correspond to the times when the wave packet excited in $|2\rangle$ passes through the potential crossing region. The transition probability of the latter case is smaller as compared with that of the former case. This is because, at the crossing region, the mean velocity of the wave packet optically excited in $|2\rangle$ is larger than that in

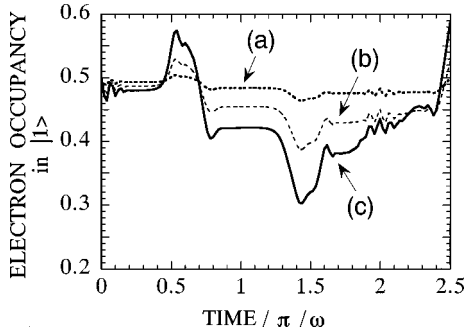

FIG. 10. Time evolution of the electron occupancy in the state $|1\rangle$, $\rho_1(t)$ $[=1-\rho_2(t)]$, for the case of the two-level excitation. (a) $T/\omega=0.5$, (b) 1.0, (c) 1.5.

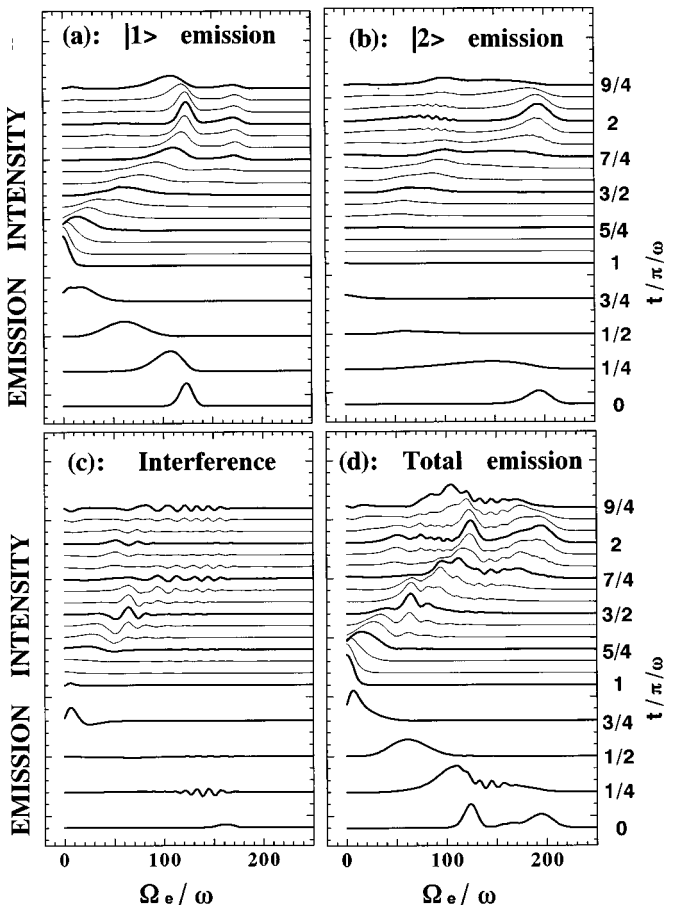

FIG. 11. Time-resolved emission spectra as a function of Ω_e for $T/\omega=1.5$ in the two-level excitation case. (a), (b), (c), and (d) are the same as Fig. 4. δ_e^{-1} is set to be $\frac{1}{4}\pi/\omega$.

$|1\rangle$ as seen in Fig. 1. This is a well-known fact given by the Landau-Zener formula.[12]

The time-resolved secondary-emission spectra for the two-level excitation case are shown in Fig. 11 as a function of Ω_e and time; (a), (b), (c), and (d) are the components of S_1, S_2, S_{12}, and S, respectively. T and δ_e^{-1} are set to be 1.5ω and $\frac{1}{4}\pi/\omega$, respectively.

Comparing S in Fig. 11(d) and that for the one-level excitation case in Fig. 4(d), we can see that both spectra have almost the same structures in the region $\Omega_e<150\omega$ and $0.5\pi/\omega\leqslant t\leqslant 1.5\pi/\omega$. This is because, in this time region, the component of the wave packet optically excited in $|2\rangle$ moves along the potential curve where it cannot make the transition to $|0\rangle$ emitting the photon as seen in Fig. 1, and hence only the transition from the photoexcited component in $|1\rangle$ takes part in the emission processes.

In the interference component of the emission in Fig. 11(c), two different types of oscillatory structures appear; one is observed in the region of $\Omega_e>130\omega$ at $t=\frac{1}{4}\pi/\omega$, $\frac{7}{4}\pi/\omega$, and $\frac{9}{4}\pi/\omega$, and the other in the vicinity of $\Omega_e=100\omega$ at $t=\frac{7}{4}\pi/\omega$, $\frac{9}{4}\pi/\omega$. The former types of oscillation have not appeared in the one-level excitation case. We have confirmed that these structures are observed even if $T=0$. Therefore, they are identified to come from the interference in the emission associated with the two components in $|1\rangle$ and $|2\rangle$ whose classical trajectories have the same phase cross at corresponding points in the energy-time domain. The latter oscillatory structures have completely inverted phases from each other and their periods become long as decreasing Ω_e. Referring the energy-time regions of the oscillatory structures in these spectra, we can conclude that the origin of the oscillation is the interference in the emitted photon associated with the following two components of the wave packet: one is created in $|1\rangle$ ($|2\rangle$) from $|2\rangle$ ($|1\rangle$) through the nonradiative transition that occurs at $t=1.6\pi/\omega$ $(2.2\pi/\omega)$, and the other is left in $|2\rangle$ ($|1\rangle$) without making the transition. The process of the interference is essentially the same as those occurring in X_5 and X_3 for the one-level excitation case discussed in Sec. III C. In this case, however, the relevant wave packets originate from the Franck-Condon state created in $|2\rangle$ by the excitation pulse.

In the total emission spectra shown in Fig. 11(d), the oscillatory structures discussed above are clearly observed in addition to the peak structures coming from the emissions, S_1 and S_2. From the analysis of the spectral structures, we are able to obtain detailed information about the dynamical processes occurring during the relaxation.

V. CONCLUSIONS

Using the model Hamiltonian together with the real-time Trotter's formula, we have studied time-resolved resonant secondary emission in the three-level electron-phonon coupled system, wherein the radiative and the nonradiative transitions are competitive each other. Analyzing the time-resolved secondary-emission spectra consisting of three components, S_1, S_2, and S_{12}, we have found that the lattice relaxation, the nonradiative transition, and the interference effects in the excited states bring about distinctive features in the emission spectra.

Finally, let us briefly discuss the processes of the optical excitation. In this work, we have studied the case where the incident pulse is a white light. As a consequence, the wave packet can travel, keeping its coherency unchanged just after photoexcitation. This is the essential factor to give interference effects in the time-resolved emission spectra. If the effects of the finite width of the incident pulse is taken into account in the optical excitation processes, the initial state excited by the incident pulse is not the Franck-Condon state and the components of the propagating wave packets relax down during the optical excitation. This will bring about new problems concerning the correlation between the photoexcitation and the dynamical processes in the excited state, which will be studied in a future work.

ACKNOWLEDGMENT

We would like to thank Professor Masaki Aihara for providing us with valuable information.

[1] M. Aihara and A. Kotani, Solid State Commun. **46**, 751 (1983).
[2] M. Hama and M. Aihara, Phys. Rev. B **38**, 1221 (1988).
[3] T. Iida and T. Higashimura, Rev. Solid State Sci. **4**, 199 (1990).
[4] H. Kono and Y. Fujimura, J. Chem. Phys. **91**, 5960 (1989).
[5] K. Nasu and Y. Kayanuma, J. Phys. Soc. Jpn. **45**, 1341 (1978).
[6] Y. Kayanuma and K. Nasu, Solid State Commun. **27**, 1371 (1978).
[7] S. Muramatsu and K. Nasu, J. Phys. C **18**, 3729 (1985).
[8] M. S. Child, *Molecular Collision Theory* (Academic, New York, 1974).
[9] H. Yagisawa, J. Phys. B **9**, 2725 (1976).
[10] M. Suzuki and K. Nasu, J. Chem. Phys. **92**, 4576 (1990).
[11] M. Suzuki, J. Chem. Phys. **105**, 1584 (1996).
[12] C. Zener, Proc. R. Soc. London, Ser. A **137**, 696 (1932).